Effect of Changing Heart Rate on the Ocular Pulse and Dynamic Biomechanical Behavior of the Optic Nerve Head

Yuejiao Jin[*1,2], Xiaofei Wang[*3], Sylvi Febriana Rachmawati Irnadiastputri[2], Rosmin Elsa Mohan[2,4], Tin Aung[4-6], Shamira A. Perera[4,5], Craig Boote[2,10], Jost B. Jonas[11], Leopold Schmetterer[4,5,7-9], Michaël J.A. Girard[2,4]

1. NUS Graduate School for Integrative Sciences and Engineering, National University of Singapore, Singapore
2. Department of Biomedical Engineering, National University of Singapore, Singapore
3. Beijing Advanced Innovation Center for Biomedical Engineering, School of Biological Science and Medical Engineering, Beihang University, Beijing, China
4. Singapore Eye Research Institute, Singapore National Eye Centre, Singapore
5. Duke-NUS Medical School, Singapore
6. Department of Ophthalmology, Yong Loo Lin School of Medicine, National University of Singapore, Singapore
7. Lee Kong Chian School of Medicine, Nanyang Technological University, Singapore
8. Department of Clinical Pharmacology, Medical University of Vienna, Austria
9. Center for Medical Physics and Biomedical Engineering, Medical University of Vienna, Austria
10. School of Optometry & Vision Sciences, Cardiff University, UK.
11. Department of Ophthalmology Medical Faculty Mannheim, Heidelberg University, Mannheim, Germany

*YJ and XW contributed equally

Word count: 4798 (Manuscript Text)

Tables: 1

Figures: 9

Corresponding Author: Michaël J. A. Girard, Ph.D.
National University of Singapore
Engineering Block 4, #04-8
4 Engineering Drive 3
Singapore 117583
mgirard@nus.edu.sg
+65 6516 5549
http://www.bioeng.nus.edu.sg/OEIL/

53 **ABSTRACT**

54 **Purpose:** To study the effect of changing heart rate on the ocular pulse and the

55 dynamic biomechanical behaviour of the optic nerve head (ONH) using a

56 comprehensive mathematical model.

57

58 **Methods:** In a finite element model of a healthy eye, a biphasic choroid consisted of

59 a solid phase with connective tissues and a fluid phase with blood, and the lamina

60 cribrosa (LC) was viscoelastic as characterized by a stress-relaxation test. We

61 applied arterial pressures at 18 ocular entry sites (posterior ciliary arteries) and

62 venous pressures at four exit sites (vortex veins). In the model, the heart rate was

63 varied from 60 bpm to 120 bpm (increment: 20 bpm). We assessed the ocular pulse

64 amplitude (OPA), pulse volume, ONH deformations and the dynamic modulus of the

65 LC at different heart rates.

66

67 **Results:** With an increasing heart rate, the OPA decreased by 0.04 mmHg for every

68 10 bpm increase in heart rate. The ocular pulse volume decreased linearly by

69 0.13 μL for every 10 bpm increase in heart rate. The storage modulus and the loss

70 modulus of the LC increased by 0.014 MPa and 0.04 MPa, respectively, for every 10

71 bpm increase in heart rate.

72

73 **Conclusions:** In our model, the OPA, pulse volume, and ONH deformations

74 decreased with an increasing heart rate, while the LC became stiffer. The effects of

75 blood pressure / heart rate changes on ONH stiffening may be of interest for

76 glaucoma pathology.

77

78

79

80

81

82

83

84

85

86

87

88

INTRODUCTION

Glaucoma is a complex, multifactorial disease. Although the pathogenic mechanism of glaucoma has still not been well understood, it has generally been accepted that various interlinked biomechanical and vascular pathways to glaucomatous injury are involved, and that these are closely related to the optic nerve head (ONH) biomechanics.[1-8] The ONH, and in particular the lamina cribrosa (LC), is a primary site of interest during the development of glaucoma since it is the region where retinal ganglion cell (RGC) axon damage occurs. Because the ONH is constantly exposed to several loads in vivo (e.g. IOP, cerebrospinal fluid pressure (CSFP), orbital fat pressure, optic nerve traction),[6, 9-13] there is a general consensus that knowing how 'robust' a ONH is could be a critical information for estimating the risk of developing glaucoma.

To date, to assess the biomechanics of the ONH in vivo, the typical approach has been to artificially manipulate IOP (e.g. with ophthalmodynamometry) while observing the resulting deformations with optical coherence tomography (OCT).[14-17] While such methods may have value from a research point of view, they may not be easily translated clinically due to discomfort during the examination of the patients. However, IOP is not constant but rather pulsatile, fluctuating constantly with the cardiac cycle. The fluctuation of IOP with the heart rate has been known as the ocular pulse and the difference between the systolic and diastolic IOP has been termed the ocular pulse amplitude (OPA). In a previous study, we proposed a framework to assess ONH biomechanics in vivo without artificially manipulating IOP. ONH deformations can indeed be measured by using the ocular pulse as the load,[18] and from such data, modelling can help us interpret these deformation data to derive stiffness estimates for the ONH.[19]

This is however a complex engineering problem: the ONH tissues are viscoelastic,[7, 20, 21] which basically means that ONH stiffness is affected by the rate of loading, or in other words, the duration of the cardiac cycle. Indeed, collagenous soft tissues typically appear stiffer when they are loaded faster. This is a protective mechanism for soft tissues to handle highly dynamic events.[7, 20] Furthermore, it has been shown clinically, that an increase in heart rate or a change in blood pressure can also affect the OPA;[22, 23] this will in turn affect the deformations of the ONH.

121   To measure the stiffness of the ONH using the ocular pulse as a natural load,
122   we believe it is critical to first build an understanding of how the heart rate and blood
123   pressure change the IOP (i.e. the OPA), and how they also affect the stiffness and
124   deformations of the ONH tissues. From a clinical point of view, if ONH tissues
125   appear stiffer, a physician should be able to tell whether this is because of a different
126   heart rate / blood pressure, or because of tissue remodelling from glaucoma. In this
127   study, we aim to build such an understanding using finite element (FE) modelling. In
128   the future, our proposed models could be combined with experimental data to
129   assess ONH stiffness in vivo.

130

131

132   **METHODS**
133   Using FE modelling, we previously modelled the origin of the ocular pulse and its
134   effect on the ONH.[19] We found that a change in arterial pressure (as that occurring
135   from diastole to systole) resulted in choroidal swelling, which in turn induced a
136   change in IOP (the OPA) due to the incompressibility of the vitreous. Both the OPA
137   and choroidal swelling were responsible for deforming the ONH tissues, and a
138   relatively large shearing of neural tissues was observed within the neuroretinal rim.
139   The vast majority of the trends we reported matched clinical and experimental data.

140   In this study, we used the same model, but we further defined the LC as a
141   viscoelastic material. Such viscoelastic properties were obtained experimentally
142   using uniaxial stress relaxation tests. Using our FE model, we then varied the heart
143   rate from 60 bpm to 120 bpm and studied its effect on: 1) the OPA, 2) the choroidal
144   pulse volume, 3) ONH deformations, and 4) LC stiffness.

145

146   **Three-Dimensional Geometry of the Ocular and Orbital Tissues**
147   The geometry of the three-dimensional eye model was adapted from our previous
148   studies.[12, 19, 24] In summary, the eye globe and optic nerve were reconstructed from
149   magnetic resonance imaging images of a heathy subject. The corneoscleral shell
150   was assumed to be spherical with an outer diameter of 24 mm and thickness of 1
151   mm. The optic nerve was composed of three tissues: the nerve tissue, the pia mater
152   and the dura mater. A generic ONH geometry was constructed and embedded within
153   the corneoscleral shell, including the scleral flange, Bruch's membrane, the LC, the
154   prelaminar tissue and the border tissue of Elschnig and Jacoby as extensions of the

155 pia mater. The model was then meshed using 67,584 eight-node hexahedrons and
156 3,024 six-node pentahedrons (Figure 1). The mesh density was numerically
157 validated through a convergence test. The whole eye was reconstructed, and
158 symmetry conditions were not applied.

159

160 **Biomechanical Properties of the Ocular Tissues**
161 The sclera was modelled as a fiber-reinforced composite, as described in our
162 previous paper.[25] The neural tissues and Bruch's membrane were modelled as
163 isotropic elastic materials. [26] The pia and dura were modelled as Yeoh materials, as
164 characterized from experiments with porcine eyes.[24] As performed in our previous
165 study, we modelled the choroid as a biphasic material comprising a solid phase and
166 a fluid phase (i.e. blood) to allow for changes in blood pressure during the cardiac
167 cycle and the movement of blood within the choroid.[19] All biomechanical parameters
168 are listed in **Table 1**.

169

170 **Viscoelastic Properties of the Lamina Cribrosa**
171 In order to characterize the response of the LC under dynamic loading such as the
172 heart rate, we studied its viscoelastic properties. Since the viscoelasticity properties
173 of the LC have not been reported in the literature yet, we conducted uniaxial stress
174 relaxation tests of the LC of seven porcine eyes.

175 Experiments were performed in accordance to the ARVO (Association for
176 Research in Vision and Ophthalmology) statement for the Use of Animals in
177 Ophthalmic and Vision Research. The experimental procedure followed the
178 previously described methodology designed for the sclera.[27, 28] In brief, seven fresh
179 porcine eyes were collected and cleaned of all extraorbital tissues. After dissecting
180 the eye and cutting the optic nerve, the retina and choroidal layers were removed. A
181 customized device was used to cut a scleral strip (orientation: inferior to superior)
182 with the LC in its center (width: 1.2 mm; Figure 2). Mineral oil was applied to the
183 specimen surface to maintain hydration. Each sample was mounted between the two
184 grips of the uniaxial tensile tester (Instron 5848; Instron. Inc., Noor wood, MA, USA)
185 with the LC exposed in the center (Figure 2c). The sample was subjected to 10
186 cycles of preconditioning at 1% strain prior to the stress relaxation test. The sample
187 was then subjected to a maximum of 5% strain at a rate of 1% per second, followed
188 by a relaxation period of 300s at constant stress. These strain levels were chosen as

189   they are typically exhibited in vivo under physiological conditions (during eye

190   movements or change in IOP).[10] The thickness measurements of the LC (mean:

191   0.628mm) were obtained by spectral-domain optical coherence tomography

192   (Spectralis OCT, Heidelberg Engineering, Heidelberg, Germany) and were used to

193   compute the tensile stress. The averaged stress values of seven porcine eyes were

194   fitted with a linear viscoelastic model incorporating a reduced relaxation function to

195   characterize the viscoelastic properties of the LC.[28] A typical stress relaxation curve

196   is shown in Figure 2d.

197

198   **Boundary and Loading conditions**

199   Two sets of boundary conditions were applied to ensure numerical stability. First, the

200   orbital apex of the optic nerve was fixed to model its connection to the optic canal.

201   Second, the eye globe was fixed near the equator on two opposite sides with four

202   nodes on each side. This was carried out to improve stability and to avoid such

203   boundary conditions from having an impact on the ONH deformations.

204   We applied a baseline IOP of 15 mmHg to the inner limiting membrane and a

205   baseline CSFP of 11.3 mmHg to the arachnoid space (Figure 3).[29] As described

206   previously, we applied prescribed fluid pressures on the choroidal layer to mimic the

207   blood flow inlets (long and short posterior ciliary arteries [PCAs]) and outlets (vortex

208   veins).[19] The arterial pressure was varied between 70.8 and 93 mmHg to mimic the

209   diastolic and systolic changes of the ophthalmic artery pressure.[30] A constant blood

210   pressure of 15 mmHg was applied at the four vortex veins exits out of the choroid.[31]

211   In our model, it was the pressure difference between the PCAs and vortex veins that

212   drove the choroidal blood flow, allowing the choroid to swell during the cardiac cycle.

213

214   **Changing the Heart Rate from 60 to 120 bpm**

215   We aimed to understand the impact of different heart rates on the ocular pulse, ONH

216   deformations, and LC stiffness. Hence, four models were implemented with the heart

217   rate ranging from 60 to 120 bpm with an increment of 20 bpm. All the boundary

218   conditions and material properties were kept constant, such that only the heart rate

219   varied.

220

221   **FE Processing to Predict the OPA, Pulse Volume, and ONH Deformations**

222   All FE models were solved with FEBIO v2.8.5 (Musculoskeletal Research

223   laboratories, University of Utah, Salt Lake City, UT, USA).[32] The OPA was estimated

224   by first assuming that the vitreous was incompressible as performed in our previous

225   study.[19] This is a reasonable assumption because the vitreous mostly consists of

226   water, which is also incompressible, and is gas-free. Therefore, the volume of the

227   vitreous body was constrained to remain constant during choroidal swelling in all our

228   simulations. Since our model aimed to reproduce choroidal swelling during the

229   cardiac cycle, such a swelling will try to deform and change the volume of the

230   vitreous body. Since the vitreous body was constrained as incompressible, an

231   internal pressure needed to be applied to maintain its volume. This pressure term is

232   an output of our model and can be understood as the OPA.

233   More specifically, each model was implemented in three steps as shown in

234   Figure 4. The initial step applied boundary conditions and loads including baseline

235   IOP, CSFP and ophthalmic arterial pressure and vortex vein pressure. During the

236   second step, a 5000s relaxation period was applied due to the viscoelasticity of the

237   LC. All the boundary conditions and loads remained unchanged. During the final step,

238   we imposed a volume constraint to the inner limiting membrane to ensure the

239   incompressibility of the vitreous.[19] The CSFP, baseline IOP and vortex vein pressure

240   were kept constant; the ophthalmic arterial pressure varied from diastole to systole

241   periodically following a sinusoidal profile for two cycles.

242   The post processing was performed using MATLAB (v2018; Mathworks,

243   Natick, MA, USA). For each model, we reported the OPA, the pulse volume, the

244   diastole-to-systole displacements of the LC and of the pre-lamina tissue. In addition,

245   we characterized the stiffness of the LC at different heart rates in the central region

246   along the radial, circumferential and longitudinal directions (Figure 5).

247

Characterizing LC Stiffness with Changing Heart Rate

249   The stiffness of the LC can be characterized by computing its dynamic modulus, as

250   typically performed for dynamic mechanical analyses.[20] Since the ocular pulse

251   induced a cyclic deformation of the LC, the LC strain 'input' can be represented as:

252   $$\varepsilon = \varepsilon_0 \sin(\omega t + \delta_\varepsilon) \tag{1}$$

253   where ε_0, δ_ε, and ω are the peak strain amplitude, strain phase shift and angular

254   frequency of the harmonic excitation, respectively. Since the LC only exhibits small

255   strains, the LC can be approximated to be linear viscoelastic.[33] Hence, the resulting

256   sinusoidal stress 'output' would differ in phase from the 'input' strain depending on
257   the viscoelastic properties of the LC, and can be expressed as:

258 $$\sigma = \sigma_0 \sin{(\omega t + \delta_\sigma)} \qquad\qquad (2)$$

259   where σ_0 and δ_σ are the peak stress amplitude and stress phase shift, respectively.
260   The phase delay between the stress and the strain due to viscoelastic effects is
261   known as the phase lag δ, i.e. the difference between δ_ε and δ_σ (Figure 6). The
262   dynamic mechanical properties of the LC can now be represented by the complex
263   dynamic modulus, consisting of the storage modulus (elastic component) and the
264   loss modulus (viscous component). It is defined as:

265 $$E^* = \frac{\sigma}{\varepsilon} = E' + iE'' \qquad\qquad (3)$$

266   where E' is the storage modulus, E'' is the loss modulus, and i the unit imaginary
267   number. The storage and loss moduli are related to the phase lag through the
268   following equations:

269 $$E' = E * \cos(\delta), \qquad\qquad (4a)$$

270 $$E'' = E * \sin(\delta) \qquad\qquad (4b)$$

271

272   For each heart rate, we computed the storage and loss moduli in the central
273   region of the LC (composed of one element). We first computed the Lagrange strain
274   and Cauchy stress tensors, and estimated the diastole-to-systole Lagrange strain
275   and Cauchy stress profiles along three directions (radial, circumferential, and
276   longitudinal). Each strain/stress profile was then fitted with equations (1-2) to
277   determine the peak strain/stress amplitudes and the phase shifts. From these data
278   we extracted the phase lag, and thus the storage and loss moduli of the LC central
279   region along 3 directions: radial, circumferential, and longitudinal.

280

281   **RESULTS**

282

283   **Effect of the Heart Rate on the Ocular Pulse**

284   For each model, the pulsating arterial pressure during the cardiac cycle
285   resulted in choroidal swelling (increase in pulse volume), which in turn increased the
286   IOP (the delta change in IOP being the OPA). The IOP and the pulse volume as
287   functions of time are shown in Figure 7 for two cycles at a heart rate of 60 bpm.

288   We also found that both the OPA and the pulse volume decreased with an

289   increasing heart rate (Figure 7). On average, the OPA and the pulse volume

290   decreased by 0.04 mmHg (2.7%) and 0.13μL (2.8%), respectively for every 10 bpm

291   heart rate increment.

292

293

294   **Effect of the Heart Rate on ONH Deformations**

295   During the cardiac cycle, the ONH moved posteriorly (diastole-to-systole) and

296   anteriorly (systole-to-diastole). The diastole-to-systole displacement of the central

297   anterior LC point was 5.8 μm at a heart rate of 60 bpm and decreased by 0.1 μm for

298   every 10 bpm heart rate increment (Figure 8a-c).

299   We also observed that the prelamina (neural tissue anterior to the lamina) and

300   the parapapillary retina moved along opposite directions during the cardiac cycle.

301   Specifically, from diastole to systole, the prelamina moved posteriorly (as highlighted

302   in red in Figure 8d), whereas the parapapillary retina (highlighted in black in Figure

303   8d) moved anteriorly. This resulted in a net shearing of the neural tissues in the

304   neuro-retinal rim. This shearing amount (difference between the prelamina

305   displacement and the parapapillary retina displacement) also decreased with an

306   increasing heart rate. On average, the shearing amount reduced by 0.12 μm for

307   every 10 bpm heart rate increment (Figure 8f).

308

309   **Effect of the Heart Rate on LC stiffness**

310   The storage and loss moduli were computed in the central region of the LC for

311   3 orientations (radial, circumferential, and longitudinal). They all followed the exact

312   same trend and all increased with an increasing heart rate. On average, the storage

313   modulus increased by 0.014 MPa, and the loss modulus by 0.04 MPa, for every 10

314   bpm heart rate increment. This indicates that the lamina cribrosa will appear stiffer

315   with a higher heart rate.

316

317

318

319

320

321

322

DISCUSSION

In this study, we used FE modelling to study the impact of the heart rate on the ocular pulse and its biomechanical impact on the ONH. Our model predicted that the OPA, pulse volume and ONH deformations decreased with an increasing heart rate. In addition, the LC became stiffer at faster heart rates. These findings may help develop technologies to finely assess the biomechanical properties of the ONH in vivo.

330

The OPA and the Pulse Volume Decreased with an Increasing Heart Rate

With an increase in heart rate, both the OPA and the pulse volume reduced when simultaneously the ophthalmic arterial and venous vein pressures were kept constant. A faster heart rate is associated with a shorter duration for each cardiac cycle, suggesting that the volume of blood being pushed into the choroid would be reduced for each pulse. Our results are also consistent with a previous clinical study,[23] in which all the subjects were fitted with cardiac pacemakers and the heart rate was altered by resetting the pacemakers. Neither IOP nor systolic-diastolic blood pressures were found to be significantly altered during the experiments, suggesting that the heart rate was one of the main contributing factor causing a reduction in OPA.

It has also been observed that a short period of dynamic exercise can also lead to a reduction in OPA and ocular pulse volume.[34-36] However, the impact of exercise is complex as it involves changes in multiple physical parameters including not only the IOP and heart rate, but also the systolic and diastolic blood pressures, and blood distribution in the body. Although heart rate and blood pressures involve separate mechanisms, exercises would induce an increase in both heart rate and blood pressures.[37] The systolic and diastolic blood pressures are related to the ocular pulse through the ocular perfusion pressure (OPP), defined as the difference between the mean blood pressure and IOP. In one study, there was a significant reduction in IOP, and an increase in OPP immediately after strenuous exercise (resting: heart rate= 68$\pm$7.9 bpm, IOP= 19.8$\pm$5.4 mmHg, OPP = 51.2$\pm$4.9 mmHg; after exercise: heart rate=125$\pm$24.9 bpm, IOP=14.3$\pm$5.0 mmHg, OPP=56.9$\pm$7.5

354   mmHg).[36] Our models could potentially be used to reproduce more complex

355   scenarios such as those.

356

357   ONH deformations and Neural Tissue Shear Decreased with an Increasing

358   Heart Rate

359   Our model predicted that ONH deformations decreased with an increasing heart rate.

360   It has been shown that isometric exercise caused a significant increase in the mean

361   arterial blood pressure and pulse rate, and decreased the fundus pulsation amplitude,

362   as measured by laser interferometry.[22] Despite changes in the mean arterial blood

363   pressure, reduced fundus pulsation amplitude may indicate a decrease in ONH

364   deformations at a faster heart rate, which is consistent with our predicted results.

365   From diastole to systole, the shearing amount refers to the anterior movement

366   of the parapapillary retina due to the choroidal expansion and the posterior ONH

367   deformation due to both choroidal swelling and the OPA. With an increase in heart

368   rate, it is expected that the shearing amount would decrease due to the reduced

369   OPA and pulse volume. This shearing phenomenon has been observed in-vivo in

370   humans using low-coherence tissue interferometry. [18]

371

372   The LC Became Stiffer with an Increasing Heart Rate

373   Our model predicted that the dynamic modulus of LC increased with an increasing

374   heart rate. Similar phenomena have also been observed in other viscoelastic

375   biological tissues such as the cornea[38, 39] intervertebral discs,[40] and other

376   biomaterials.[41] The dynamic modulus characterizes the stiffness of a material in

377   response to dynamic loading, and it can differ from its static behaviour since

378   viscoelastic materials typically become more rigid with a faster loading rate.[38, 39] The

379   static modulus describes the elasticity of a tissue at 'equilibrium', whereas the

380   dynamic modulus provides information about the instant stiffness of a material. For

381   instance, for the cornea, the dynamic properties are likely dominated by the

382   rearrangement of the extracellular matrix (mainly through diffusion of water) upon

383   changes in stress, whereas the static properties are more closely related to the

384   collagen structure.[42] Histological studies have shown that the morphology of the LC,

385   as a porous, reticulated and multi-lamellar sieve-like structure, mainly comprises of

386   laminar beams consisting of elastin fibres and collagen fibrils (type I and III).[43] Hence,

387   it is likely that the dynamic and static responses of the LC are also dominated by

388   different components, and both may change differently during the progression and

389   development of glaucoma.

390

391   **Clinical Relevance to Glaucoma Pathogenesis**

392   At first view, a faster heart rate may be beneficial for the eye. First, it resulted in a

393   smaller OPA and hence smaller ONH deformations. A larger deformation would yield

394   larger stain/stress fluctuations within the LC, which may have an impact on the

395   retinal ganglion cell axons and the vascular capillaries. This is also consistent with

396   the fact that a larger OPA has been observed in chronic angle-closure glaucoma and

397   suspected open-angle glaucoma subjects.[44]

398   Second, a faster heart rate also resulted in lower neural tissue shear, which

399   may limit axonal damage in the neuroretinal rim region.[45-47] As discussed in our

400   previous work, repeated shearing of axons in the neuroretinal rim region could

401   potentially contribute to axonal damage. The neuroretinal rim is indeed a region that

402   exhibits a mechanical discontinuity: it is where RGC axons follow a sharp turn to

403   enter the disc. In this region, a reduction in Bruch's-membrane-opening minimum-

404   rim-width (BMO-MRW) has been observed clinically in glaucoma and in elderly

405   individuals.[45-50] Hence, decreasing shearing with a faster heart rate may be seen as

406   'mechanically protective'.

407   Third, the LC was found to stiffen with an increasing heart rate, which could

408   provide better support to the RGCs and vasculatures. Pseudoexfoliation (PEX)

409   syndrome is a systemic disorder of the elastic fiber system which can lead to PEX

410   glaucoma. It has been reported that the stiffness of the LC in PEX eyes is 40% less

411   than that in normal eyes as evaluated by atomic force microscopy.[51] This decrease

412   in LC stiffness may increase susceptibility to IOP-induced glaucomatous optic nerve

413   damage as observed in PEX eyes, and thus, dynamic stiffening of the LC may also

414   be seen as beneficial.

415   However, the situation may be more complex as the effects of dynamic

416   loading at the cellular level has remained elusive yet. The response of cells to

417   deformation is dependent on both the magnitude and the rate of mechanical strain.

418   Some studies have shown that short-term strain or stress variations can lead to

419   cellular injury in neurons and neuron-like cells.[52-54] Future research is required to

420   better understand the link between dynamic loading and RGC axonal injury at the

421   micro or cellular scale.

422

Understanding The Clinical Implications of LC Stiffening

424 During the development and progression of glaucoma, the connective tissues of the
425 ONH undergo constant remodelling (including stiffening in the moderate/severe
426 stages) and extensive structural changes.[55] The extracellular matrix remodelling are
427 usually characterized by fibrotic changes associated with cellular and molecular
428 events such as myofibroblast activation that could drive further tissue fibrosis and
429 stiffening.[56] However, as discussed herein, the LC also gets stiffer with an increased
430 heart rate. Ex vivo strain measurement shows that the stiffness of the LC increases
431 with age.[57] It is believed that the change in LC stiffness due to the change in heart
432 rate and aging involves different mechanisms. Our results only reflect the short-term
433 impact of a raised heart rate and we do not know whether the stiffening of the lamina
434 will become chronic or whether other homeostatic mechanisms might reverse these
435 changes in the longer term. If an increase in dynamic LC stiffness is proved to be
436 beneficial, it is possible to modulate heart rate in the longer term via pharmocologial
437 means. Finally, it is important to note that, while assessing the material properties of
438 the LC from the ocular pulse, physicians should be able to distinguish whether a
439 change in LC stiffness is because of a different heart rate/blood pressure, or
440 because of tissue remodelling. This information may be helpful to predict glaucoma
441 progression.

Limitations

443 Our study has several limitations. First, our model did not consider the regional
444 variations in the scleral thickness and stiffness, which are known to exist in monkeys,
445 canines, and humans. [20, 58, 59] The regional variations may affect the prediction of the
446 OPA.

447 Second, the choroid was simplified and modelled as a biphasic material,
448 consisting of a porous solid phase (connective tissues) and a fluid phase (blood). In
449 addition, the permeability of the choroid was approximated grossly from the vascular
450 resistance, the average diameter of the choroid and the blood viscosity. [19] The
451 complex microvasculature architecture, as well as the blood flow of the choroid,
452 cannot be fully captured by this description. For instance, the segmental distribution
453 of PCAs[60] and the autoregulatory capacity of the choroid [22, 61] were not taken into
454 account in our model. Furthermore, the PCAs and vortex veins were not modelled
455 explicitly but represented by prescribed fluid pressures. Future work may need to

456   assess the permeability of the choroid experimentally and also consider more
457   complex material models to better describe the behaviour of the pulsatile choroidal
458   blood flow.

459   Third, our model did not account for the blood circulation within the LC and
460   other pulsatile components including those from the retina, central retinal artery and
461   the CSFP. These pulsations may affect the LC deformations as well. The pulsation
462   of the CSFP is phase-shifted with respect to the ocular pulse, such that the CSFP
463   peak occurs slightly before that of the IOP.[62, 63] The phase difference between the
464   IOP and CSFP may lead to dynamic fluctuations of the translaminar pressure
465   gradient, resulting in different ONH deformation profiles. The contribution of these
466   pulsatile components may be important and should be considered in future studies.

467   Fourth, the geometry of the eye was constructed from a single eye model and
468   the dimensions of the ONH were taken as average measurements from the literature.
469   However, the ocular and ONH geometries can vary widely across individuals and
470   thus may influence the predicted ocular pulse significantly. In our model, the retina,
471   choroid and BM were simplified as a uniform layer throughout the eye. We aim to
472   take regional variations in tissue thickness into consideration in future work.

473   Fifth, we experimentally measured the viscoelastic material properties of the
474   porcine LC in this study. It is possible that the LC exhibits different viscoelastic
475   properties across species. In addition, the LC was simplified as an isotropic and
476   homogeneous material; the complicated laminar microarchitecture was not taken into
477   account. Micro-level modelling of the laminar beams predicted higher strain and
478   stress than those predicted by macro-scale models of the ONH.[64] The mean strain of
479   the laminar beams varies greatly across different nonhuman primates and depends
480   on the 3D geometry of each eye's ONH connective tissues.[64, 65] Models
481   incorporating the micro-level laminar beams may be considered in the future.

482   Sixth, for simplicity and as a first approach, we only modelled the
483   viscoelasticity of the LC and not that of other tissues such as the choroid and the
484   sclera. We focused on the LC only as it is a tissue that has been observed under
485   dynamic loading[18] and because it plays a critical role in glaucoma as the main site of
486   damage. More complex models will be needed in the future to better understand how
487   scleral and choroidal viscoelasticity could interact with the LC.

488   Seventh, the results shown only reflect the short-term impact of a raised heart
489   rate and we do not know whether the stiffening of the lamina will become chronic or

490   whether other homeostatic mechanisms might reverse these changes in the longer
491   term.

492   Eighth, the LC was modelled as a uniform structure. We did not take into
493   account potential differences in the anatomy and biomechanical properties of the
494   various layers of the LC, nor did we consider lateral movements of the LC in
495   dependence of changes of the examined parameters and in dependence of the
496   obliqueness of the optic nerve canal and the spatial relationship between Bruch´s
497   membrane opening and the lamina cribrosa position. [66, 67]

498   **Conclusions**

499   In this study, we used FE modelling to study the ocular pulse and the impact of the
500   heart rate on ONH deformations. We found that the OPA, the pulse volume the ONH
501   deformation reduce at a faster heart rate. Our models also indicated that the LC
502   becomes stiffer with increasing heart rate. These results will help us develop
503   technology to assess the biomechanics of the ONH in vivo by using the ocular pulse
504   as a natural load.

505

506
507
508
509
510
511
512
513
514
515
516
517
518
519
520
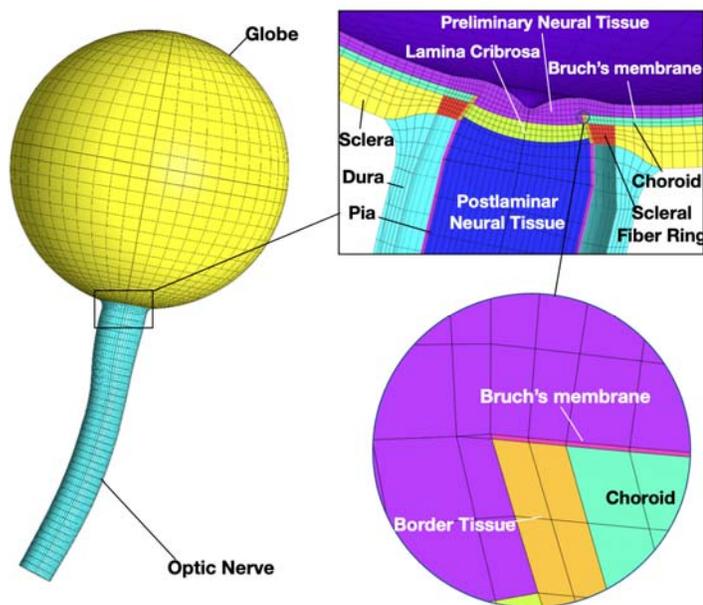521
522
523
524
525
526
527
528
529
530
531

532
533
534
535
536
537
538
539
540
541
542
543
544 **Figures and Tables**
545

546
547 **Figure 1.** Reconstructed geometry and FE mesh of the whole eye model adopted
548 from Jin.[19] ONH structures (including the LC, sclera, neural tissues, choroid, BM,
549 border tissue, pia and dura) were reconstructed using average measurements from
550 the literature.[9, 19, 24, 26, 68]

551
552
553
554
555
556
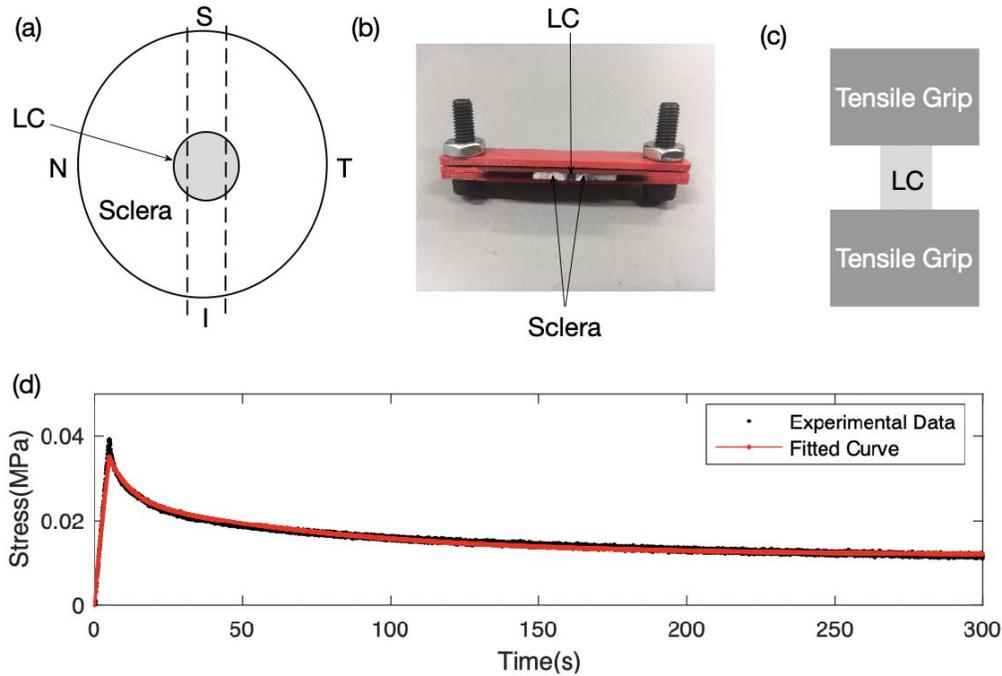
557
558 **Figure 2.** (a) Schematic showing the scleral strip with the LC in its center. The
559 uniaxial tensile specimen was obtained by using a customized device (shown in b) to
560 obtain a fixed width of 1.2 mm. It was then clamped between the tensile grips (shown
561 in c) with the LC exposed in its centre. (d) A typical stress relaxation experimental
562 test dataset for an LC sample fitted with a linear viscoelastic model curve.[28]
563
564

565
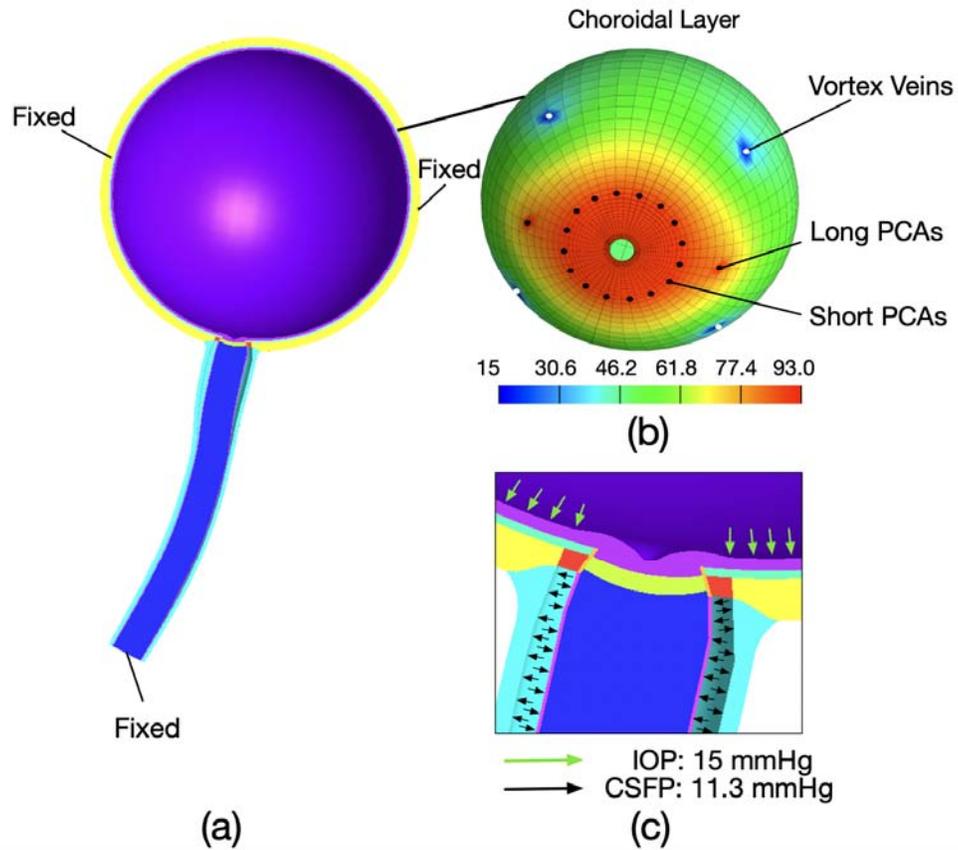
566
567
568 **Figure 3**: (a) Half eye geometry and boundary conditions: fixed optic nerve at the
569 orbital apex and fixed sclera nodes near the equator on two opposite sides. (b)
570 Choroidal with the nodes where arterial blood pressure (short and long PCAs) and
571 venous blood pressures (vortex veins) were applied. (c) ONH region illustrating the
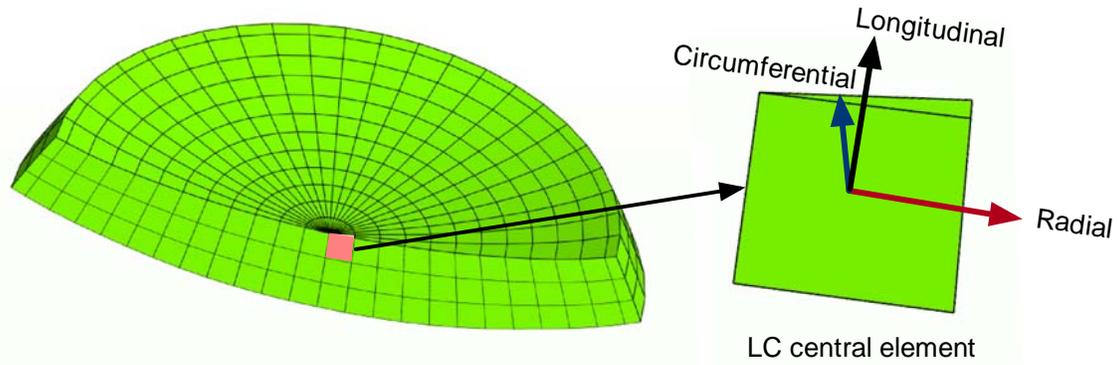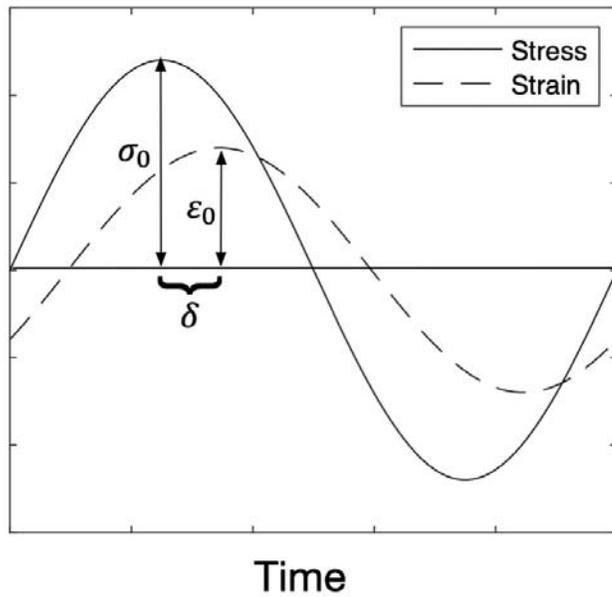572 pressure loads (IOP, CSFP) applied in each model.

573   .

574
575
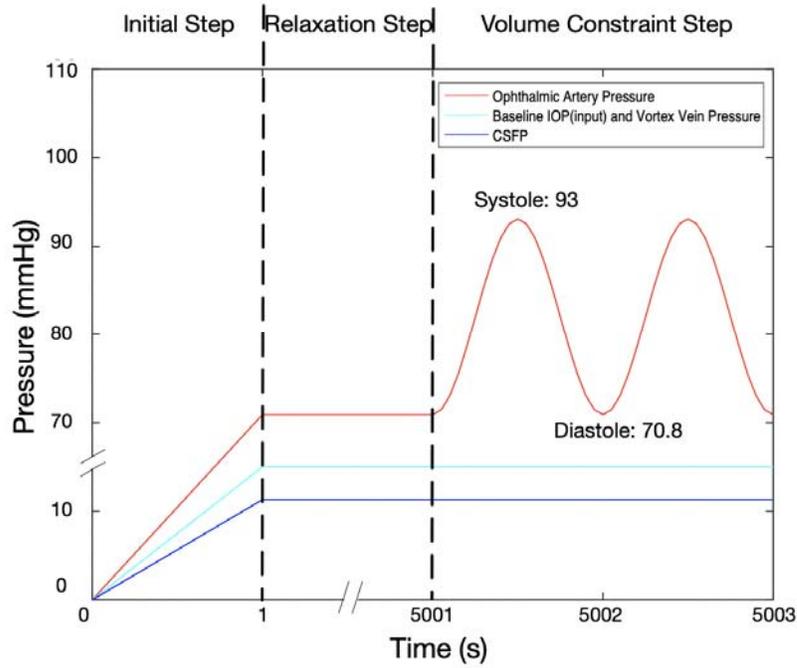
Figure 4. Profiles of different pressure loads.

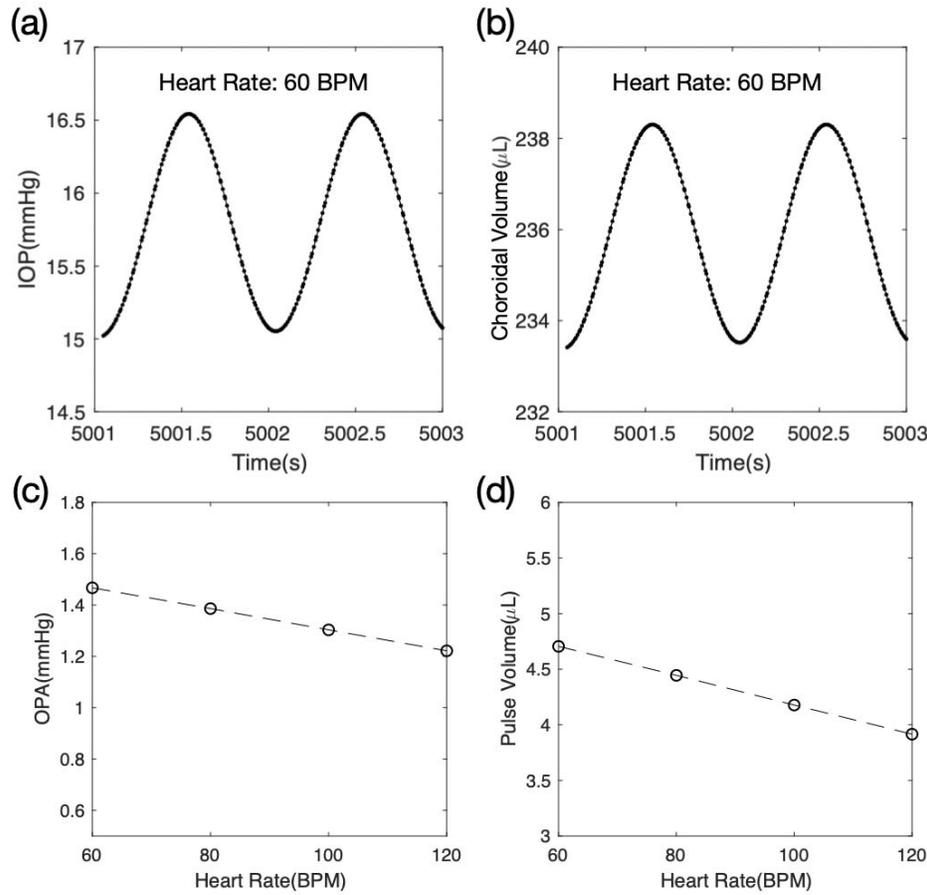**Figure 5**: Cross-section of the LC illustrating the local coordinates (radial, circumferential and longitudinal) for one central element.
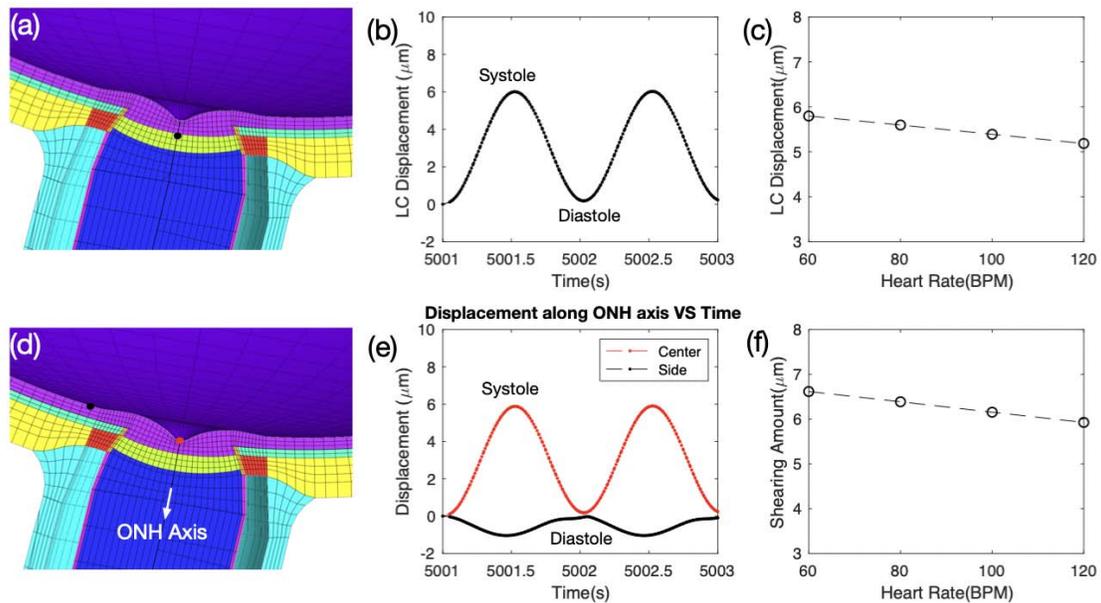

Figure 6. Schematic representation of the strain and stress profiles as a function of time in calculating the dynamic properties of the LC.

Figure 7. (a,b) IOP and choroidal volume over two cycles at a heart rate of 60 BPM.
(c,d) Change of the OPA and the pulse volume (PV) with heart rate.

Figure 8. (a) Cross-section of the ONH highlighting the center of the LC and (b) the displacement of the LC center. (c) Change of the LC displacement with increasing heart rate. (d,e) Cross-section of the ONH and the radial displacement of the highlighted points (red: center of prelaminar; black: a point on the retinal surface located 0.65 mm away from BMO) over two cardiac cycles. (f) Change of the shearing amount with heart rate.
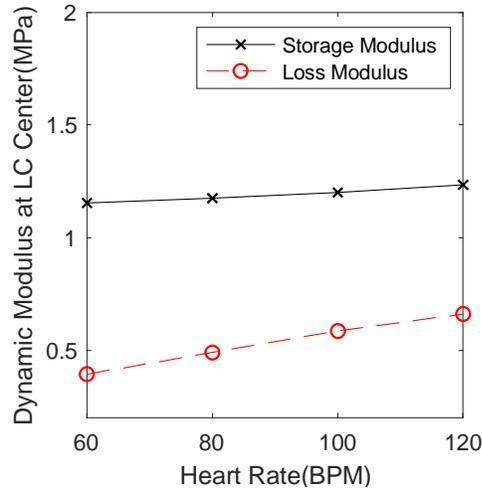
Figure 9. Change of the storage and loss moduli of the LC center with the heart rate.

660 **TABLES**

661 **Table 1.** Tissue biomechanical properties used for all models

Tissue	Constitutive Model	Biomechanical Properties	References
Sclera	Mooney-Rivlin Von Mises distributed fibers	c1 = 0.285 MPa c3 = 0.0137 MPa c4 = 658.125 kf = 2 (scleral ring) kf = 0 (other region of sclera) θ_p: preferred fiber orientation	Girard et al.[25]
LC	Viscoelastic	Instantaneous modulus = 8.49 MPa Equilibrium modulus = 0.49 MPa Long-term time constant = 272 s Short-term time constant = 8.33 s	Porcine tissue experiment (this study)
Neural tissue	Isotropic elastic	Elastic modulus = 0.03 MPa Poisson's ratio = 0.49	Miller[69]
BM	Isotropic elastic	Elastic modulus = 10.79 MPa Poisson's ratio = 0.49	Chan et al.[70]
Choroid	Biphasic	solid volume fraction: 0.55 Solid matrix: Neo-Hookean Elastic modulus = 0.06 MPa Poisson's ratio = 0 Permeability: 45037 mm^2/MPa.s	Jin et al[19]
Dura	Yeoh model	C1 = 0.1707 MPa C2 = 4.2109 MPa C3 = -4.9742 MPa	Wang et al.[24]
Pia	Yeoh model	C1 = 0.1707 MPa C2 = 4.2109 MPa C3 = -4.9742 MPa	Wang et al.[24]

Border Tissue	Isotropic elastic	Elastic modulus = 10.79MPa Poisson's ratio = 0.49	Chan et al.[70]

662
663
664   References
665

666   1.   Abegão Pinto L, Willekens K, Van Keer K, et al. Ocular blood flow in
667   glaucoma – the Leuven Eye Study. *Acta Ophthalmologica* 2016;94:592-598.
668   2.   Coudrillier B, Tian J, Alexander S, Myers KM, Quigley HA, Nguyen TD.
669   Biomechanics of the human posterior sclera: age- and glaucoma-related changes
670   measured using inflation testing. *Invest Ophthalmol Vis Sci* 2012;53:1714-1728.
671   3.   Ethier CR. Scleral biomechanics and glaucoma—a connection? *Canadian
672   Journal of Ophthalmology / Journal Canadien d'Ophtalmologie* 2006;41:9-14.
673   4.   Girard MJ, Strouthidis NG, Desjardins A, Mari JM, Ethier CR. In vivo optic
674   nerve head biomechanics: performance testing of a three-dimensional tracking
675   algorithm. *Journal of the Royal Society, Interface* 2013;10:20130459.
676   5.   Burgoyne CF, Downs JC, Bellezza AJ, Suh JK, Hart RT. The optic nerve head
677   as a biomechanical structure: a new paradigm for understanding the role of IOP-
678   related stress and strain in the pathophysiology of glaucomatous optic nerve head
679   damage. *Progress in retinal and eye research* 2005;24:39-73.
680   6.   Downs JC. Optic nerve head biomechanics in aging and disease.
681   *Experimental eye research* 2015;133:19-29.
682   7.   Downs JC, Roberts MD, Burgoyne CF. The Mechanical Environment of the
683   Optic Nerve Head in Glaucoma. *Optometry and vision science : official publication of
684   the American Academy of Optometry* 2008;85:425-435.
685   8.   Girard MJ, Suh JK, Bottlang M, Burgoyne CF, Downs JC. Biomechanical
686   changes in the sclera of monkey eyes exposed to chronic IOP elevations. *Invest
687   Ophthalmol Vis Sci* 2011;52:5656-5669.
688   9.   Sigal IA, Flanagan JG, Tertinegg I, Ethier CR. Predicted extension,
689   compression and shearing of optic nerve head tissues. *Exp Eye Res* 2007;85:312-
690   322.
691   10.   Wang X, Beotra MR, Tun TA, et al. In Vivo 3-Dimensional Strain Mapping
692   Confirms Large Optic Nerve Head Deformations Following Horizontal Eye
693   Movements. *Investigative Ophthalmology & Visual Science* 2016;57:5825-5833.
694   11.   Jonas JB, Wang N, Yang D, Ritch R, Panda-Jonas S. Facts and myths of
695   cerebrospinal fluid pressure for the physiology of the eye. *Progress in retinal and eye
696   research* 2015;46:67-83.
697   12.   Wang X, Fisher LK, Milea D, Jonas JB, Girard MJ. Predictions of Optic Nerve
698   Traction Forces and Peripapillary Tissue Stresses Following Horizontal Eye
699   Movements. *Invest Ophthalmol Vis Sci* 2017;58:2044-2053.
700   13.   Girard MJ, Beotra MR, Chin KS, et al. In Vivo 3-Dimensional Strain Mapping
701   of the Optic Nerve Head Following Intraocular Pressure Lowering by Trabeculectomy.
702   *Ophthalmology* 2016;123:1190-1200.
703   14.   Agoumi Y, Sharpe GP, Hutchison DM, Nicolela MT, Artes PH, Chauhan BC.
704   Laminar and prelaminar tissue displacement during intraocular pressure elevation in
705   glaucoma patients and healthy controls. *Ophthalmology* 2011;118:52-59.
706   15.   Fazio MA, Johnstone JK, Smith B, Wang L, Girkin CA. Displacement of the
707   Lamina Cribrosa in Response to Acute Intraocular Pressure Elevation in Normal

708 Individuals of African and European Descent. *Invest Ophthalmol Vis Sci*
709 2016;57:3331-3339.
710 16.   Girard MJ, Tun TA, Husain R, et al. Lamina cribrosa visibility using optical
711 coherence tomography: comparison of devices and effects of image enhancement
712 techniques. *Invest Ophthalmol Vis Sci* 2015;56:865-874.
713 17.   Motschmann M, Muller C, Kuchenbecker J, et al. Ophthalmodynamometry: a
714 reliable method for measuring intracranial pressure. *Strabismus* 2001;9:13-16.
715 18.   Dragostinoff N, Werkmeister RM, Klaizer J, Groschl M, Schmetterer L. Time
716 course and topographic distribution of ocular fundus pulsation measured by low-
717 coherence tissue interferometry. *J Biomed Opt* 2013;18:121502.
718 19.   Jin Y, Wang X, Zhang L, et al. Modeling the Origin of the Ocular Pulse and Its
719 Impact on the Optic Nerve HeadModeling the Origin of the Ocular Pulse.
720 *Investigative Ophthalmology & Visual Science* 2018;59:3997-4010.
721 20.   Palko JR, Pan X, Liu J. Dynamic testing of regional viscoelastic behavior of
722 canine sclera. *Exp Eye Res* 2011;93:825-832.
723 21.   Pavlatos E, Ma Y, Clayson K, Pan X, Liu J. Regional deformation of the optic
724 nerve head and peripapillary sclera during IOP elevation. *Investigative
725 ophthalmology & visual science* 2018;59:3779-3788.
726 22.   Kiss B, Dallinger S, Polak K, Findl O, Eichler HG, Schmetterer L. Ocular
727 hemodynamics during isometric exercise. *Microvasc Res* 2001;61:1-13.
728 23.   Trew DR, James CB, Thomas SHL, Sutton R, Smith SE. Factors influencing
729 the ocular pulse — the heart rate. *Graefe's Archive for Clinical and Experimental
730 Ophthalmology* 1991;229:553-556.
731 24.   Wang X, Rumpel H, Lim WE, et al. Finite Element Analysis Predicts Large
732 Optic Nerve Head Strains During Horizontal Eye Movements. *Invest Ophthalmol Vis
733 Sci* 2016;57:2452-2462.
734 25.   Girard MJ, Suh JK, Bottlang M, Burgoyne CF, Downs JC. Scleral
735 biomechanics in the aging monkey eye. *Invest Ophthalmol Vis Sci* 2009;50:5226-
736 5237.
737 26.   Sigal IA, Flanagan JG, Ethier CR. Factors influencing optic nerve head
738 biomechanics. *Invest Ophthalmol Vis Sci* 2005;46:4189-4199.
739 27.   Downs JC, Suh JK, Thomas KA, Bellezza AJ, Hart RT, Burgoyne CF.
740 Viscoelastic material properties of the peripapillary sclera in normal and early-
741 glaucoma monkey eyes. *Invest Ophthalmol Vis Sci* 2005;46:540-546.
742 28.   Downs JC, Suh JK, Thomas KA, Bellezza AJ, Burgoyne CF, Hart RT.
743 Viscoelastic characterization of peripapillary sclera: material properties by quadrant
744 in rabbit and monkey eyes. *J Biomech Eng* 2003;125:124-131.
745 29.   Linden C, Qvarlander S, Johannesson G, et al. Normal-Tension Glaucoma
746 Has Normal Intracranial Pressure: A Prospective Study of Intracranial Pressure and
747 Intraocular Pressure in Different Body Positions. *Ophthalmology* 2017.
748 30.   Hayreh SS, Edwards J. Ophthalmic arterial and venous pressures. Effects of
749 acute intracranial hypertension. *The British journal of ophthalmology* 1971;55:649-
750 663.
751 31.   Ethier CR, Johnson M, Ruberti J. Ocular biomechanics and biotransport.
752 *Annual review of biomedical engineering* 2004;6:249-273.
753 32.   Maas SA, Ellis BJ, Ateshian GA, Weiss JA. FEBio: Finite Elements for
754 Biomechanics. *Journal of Biomechanical Engineering* 2012;134:11005.
755 33.   Fung YC. *Biomechanics: Mechanical Properties of Living Tissues*: Springer
756 New York; 2013.

757   34.   Read S, Collins M. The short-term influence of exercise on axial length and
758   intraocular pressure. *Eye* 2011;25:767.
759   35.   Lovasik JV, Kergoat H. Consequences of an increase in the ocular perfusion
760   pressure on the pulsatile ocular blood flow. *Optom Vis Sci* 2004;81:692-698.
761   36.   Price EL, Gray LS, Humphries L, Zweig C, Button NF. Effect of exercise on
762   intraocular pressure and pulsatile ocular blood flow in a young normal population.
763   *Optom Vis Sci* 2003;80:460-466.
764   37.   Miyai N, Arita M, Miyashita K, Morioka I, Shiraishi T, Nishio I. Blood pressure
765   response to heart rate during exercise test and risk of future hypertension.
766   *Hypertension* 2002;39:761-766.
767   38.   Boyce B, Jones R, Nguyen T, Grazier J. Stress-controlled viscoelastic tensile
768   response of bovine cornea. *Journal of biomechanics* 2007;40:2367-2376.
769   39.   Elsheikh A, Wang D, Brown M, Rama P, Campanelli M, Pye D. Assessment
770   of corneal biomechanical properties and their variation with age. *Current eye
771   research* 2007;32:11-19.
772   40.   Race A, Broom ND, Robertson P. Effect of loading rate and hydration on the
773   mechanical properties of the disc. *Spine* 2000;25:662-669.
774   41.   Tirella A, Mattei G, Ahluwalia A. Strain rate viscoelastic analysis of soft and
775   highly hydrated biomaterials. *Journal of biomedical materials research Part A*
776   2014;102:3352-3360.
777   42.   Kling S, Bekesi N, Dorronsoro C, Pascual D, Marcos S. Corneal viscoelastic
778   properties from finite-element analysis of in vivo air-puff deformation. *PloS one*
779   2014;9:e104904.
780   43.   Tan NY, Koh V, Girard MJ, Cheng CY. Imaging of the lamina cribrosa and its
781   role in glaucoma: a review. *Clinical & experimental ophthalmology* 2018;46:177-188.
782   44.   Cheng L, Ding Y, Duan X, Wu Z. Ocular pulse amplitude in different types of
783   glaucoma using dynamic contour tonometry: Diagnosis and follow‐up of glaucoma.
784   *Experimental and Therapeutic Medicine* 2017;14:4148-4152.
785   45.   Chauhan BC, Danthurebandara VM, Sharpe GP, et al. Bruch's Membrane
786   Opening Minimum Rim Width and Retinal Nerve Fiber Layer Thickness in a Normal
787   White Population: A Multicenter Study. *Ophthalmology* 2015;122:1786-1794.
788   46.   Chauhan BC, O'Leary N, Almobarak FA, et al. Enhanced detection of open-
789   angle glaucoma with an anatomically accurate optical coherence tomography-
790   derived neuroretinal rim parameter. *Ophthalmology* 2013;120:535-543.
791   47.   Tun TA, Sun CH, Baskaran M, et al. Determinants of optical coherence
792   tomography-derived minimum neuroretinal rim width in a normal Chinese population.
793   *Invest Ophthalmol Vis Sci* 2015;56:3337-3344.
794   48.   Gmeiner JM, Schrems WA, Mardin CY, Laemmer R, Kruse FE, Schrems-
795   Hoesl LM. Comparison of Bruch's membrane opening minimum rim width and
796   peripapillary retinal nerve fiber layer thickness in early glaucoma assessment.
797   *Investigative Ophthalmology & visual science* 2016;57:OCT575-OCT584.
798   49.   Danthurebandara VM, Sharpe GP, Hutchison DM, et al. Enhanced structure–
799   function relationship in glaucoma with an anatomically and geometrically accurate
800   neuroretinal rim measurement. *Investigative ophthalmology & visual science*
801   2015;56:98-105.
802   50.   Fortune B, Yang H, Strouthidis NG, et al. The effect of acute intraocular
803   pressure elevation on peripapillary retinal thickness, retinal nerve fiber layer
804   thickness, and retardance. *Invest Ophthalmol Vis Sci* 2009;50:4719-4726.
805   51.   Braunsmann C, Hammer CM, Rheinlaender J, Kruse FE, Schäffer TE,
806   Schlötzer-Schrehardt U. Evaluation of lamina cribrosa and peripapillary sclera

807 stiffness in pseudoexfoliation and normal eyes by atomic force microscopy.
808 *Investigative ophthalmology & visual science* 2012;53:2960-2967.
809 52. Wostyn P, De Groot V, Audenaert K, De Deyn PP. Are intracranial pressure
810 fluctuations important in glaucoma? *Medical hypotheses* 2011;77:598-600.
811 53. McMonnies CW. The interaction between intracranial pressure, intraocular
812 pressure and lamina cribrosal compression in glaucoma. *Clinical & experimental*
813 *optometry* 2016;99:219-226.
814 54. Edwards ME, Wang SS, Good TA. Role of viscoelastic properties of
815 differentiated SH-SY5Y human neuroblastoma cells in cyclic shear stress injury.
816 *Biotechnology progress* 2001;17:760-767.
817 55. Grytz R, Girkin CA, Libertiaux V, Downs JC. Perspectives on biomechanical
818 growth and remodeling mechanisms in glaucoma. *Mechanics research*
819 *communications* 2012;42:92-106.
820 56. Liu B, McNally S, Kilpatrick JI, Jarvis SP, O'Brien CJ. Aging and ocular tissue
821 stiffness in glaucoma. *Survey of ophthalmology* 2018;63:56-74.
822 57. Albon J, Purslow PP, Karwatowski WS, Easty DL. Age related compliance of
823 the lamina cribrosa in human eyes. *British Journal of Ophthalmology* 2000;84:318-
824 323.
825 58. Coudrillier B, Boote C, Quigley HA, Nguyen TD. Scleral anisotropy and its
826 effects on the mechanical response of the optic nerve head. *Biomechanics and*
827 *modeling in mechanobiology* 2013;12:941-963.
828 59. Coudrillier B, Campbell IC, Read AT, et al. Effects of Peripapillary Scleral
829 Stiffening on the Deformation of the Lamina Cribrosa. *Investigative Ophthalmology &*
830 *Visual Science* 2016;57:2666-2677.
831 60. Hayreh SS. Posterior ciliary artery circulation in health and disease: the
832 Weisenfeld lecture. *Invest Ophthalmol Vis Sci* 2004;45:749-757; 748.
833 61. Polska E, Simader C, Weigert G, et al. Regulation of choroidal blood flow
834 during combined changes in intraocular pressure and arterial blood pressure. *Invest*
835 *Ophthalmol Vis Sci* 2007;48:3768-3774.
836 62. Morgan WH, Hazelton ML, Yu D-Y. Retinal venous pulsation: Expanding our
837 understanding and use of this enigmatic phenomenon. *Progress in retinal and eye*
838 *research* 2016;55:82-107.
839 63. Morgan WH, Lind CRP, Kain S, Fatehee N, Bala A, Yu D-Y. Retinal Vein
840 Pulsation Is in Phase with Intracranial Pressure and Not Intraocular Pressure.
841 *Investigative Ophthalmology & Visual Science* 2012;53:4676-4681.
842 64. Roberts MD, Grau V, Grimm J, et al. Remodeling of the connective tissue
843 microarchitecture of the lamina cribrosa in early experimental glaucoma.
844 *Investigative ophthalmology & visual science* 2009;50:681-690.
845 65. Downs J, Roberts M, Burgoyne C, Hart R. Finite element modeling of the
846 lamina cribrosa microstructure in normal and early glaucoma monkey eyes.
847 *Investigative Ophthalmology & Visual Science* 2007;48:3301-3301.
848 66. Wang YX, Zhang Q, Yang H, Chen JD, Wang N, Jonas JB. Lamina cribrosa
849 pore movement during acute intraocular pressure rise. *British Journal of*
850 *Ophthalmology* 2019;bjophthalmol-2019-314016.
851 67. Zhang Q, Xu L, Wei WB, Wang YX, Jonas JB. Size and Shape of Bruch's
852 Membrane Opening in Relationship to Axial Length, Gamma Zone, and Macular
853 Bruch's Membrane Defects. *Investigative Ophthalmology & Visual Science*
854 2019;60:2591-2598.

855   68.   Sigal IA, Grimm JL, Jan NJ, Reid K, Minckler DS, Brown DJ. Eye-specific
856   IOP-induced displacements and deformations of human lamina cribrosa. *Invest*
857   *Ophthalmol Vis Sci* 2014;55:1-15.
858   69.   Miller K. Constitutive model of brain tissue suitable for finite element analysis
859   of surgical procedures. *Journal of biomechanics* 1999;32:531-537.
860   70.   Chan WH, Hussain AA, Marshall J. Youngs Modulus of Bruchs Membrane:
861   Implications for AMD. *Investigative Ophthalmology & Visual Science* 2007;48:2187-
862   2187.
863